ENERGY MINIMIZATION FOR LIQUID CRYSTAL EQUILIBRIUM CONFIGURATIONS WITH APPLIED ELECTRIC FIELDS

J. H. ADLER, T. J. ATHERTON, **D. B. EMERSON**, S. P. MACLACHLAN

Abstract. This paper outlines an energy-minimization finite-element approach to the computational modeling of equilibrium configurations for nematic liquid crystals with applied electric fields. The method targets minimization of system free energy based on the electrically augmented Frank-Oseen free energy model. The Hessian, resulting from the linearization of the first-order optimality conditions, is shown to be invertible when discretized by a mixed finite-element method under certain assumptions. This implies that the intermediate discrete linearizations are well-posed. Two numerical experiments are performed. The first compares the algorithm's solution of a classical Freedericksz transition problem to the known analytical solution and demonstrates the convergence of the algorithm to the true solution. The second experiment targets a problem with more complicated boundary conditions, simulating a nano-patterned surface. The algorithm accurately handles heterogeneous constant coefficients and efficiently resolves configurations resulting from classical and complicated boundary conditions relevant in ongoing research.

1. Introduction

Liquid crystals are substances that possess mesophases with properties intermediate between liquids and crystals, existing at different temperatures or solvent concentrations. The discovery of liquid crystals is attributed to Reinitzer in 1888 [25]. The focus of this paper is on nematic liquid crystal phases, which are formed by rod-like molecules that self-assemble into an ordered structure, such that the molecules tend to align along a preferred orientation. The preferred average direction at any point in a domain Ω is known as the director, denoted $\mathbf{n}(x, y, z) = (n_1, n_2, n_3)^T$. The director is taken to be of unit length at every point and headless, that is $\mathbf{n}$ and $-\mathbf{n}$ are indistinguishable, reflecting the observed symmetry of the phase.

In addition to their self-structuring properties, nematic liquid crystals are dielectrically active. Thus, their configurations are affected by electric fields. Moreover, since these materials are birefringent, with refractive indices that depend on the polarization of light, they can be used to control the propagation of light through a nematic structure. These traits have led, and continue to lead, to important discoveries in display technologies and beyond [18]. Thorough overviews of liquid crystal physics are found in [7, 11, 27].

Many mathematical and computational models of liquid crystal continuum theory lead to complicated systems involving unit length constrained vector fields. Currently, the complexity of such systems has restricted the existence of known analytical solutions to simplified geometries in one (1-D) or two dimensions (2-D), often under strong simplifying assumptions. When coupled with electric fields and other effects, far fewer analytical solutions exist, even in 1-D [27]. In addition, associated systems of partial differential equations, such as the equilibrium equations [12, 27], suffer from non-unique solutions, which must be distinguished via energy arguments. Due to such difficulties, efficient, theoretically supported, numerical approaches to the modeling of nematic liquid crystals under free elastic and augmented electric effects are of great importance. A number of computational techniques for liquid crystal equilibrium and dynamics problems exist [20, 21, 27, 29], including least-squares finite-element methods [2] and discrete Lagrange multiplier approaches with simplifying assumptions [17, 24].

In this paper, we propose a method that directly targets energy minimization in the continuum, via Lagrange multiplier theory on Banach spaces, to resolve liquid crystal equilibrium configurations in the presence of applied electric fields. The approach is derived absent the often used one-constant approximation [8, 24, 27, 29]; that is, the method described here, and the accompanying theory, are applicable for a wide range of physical parameters. This allows for significantly improved modeling of physical phenomena not captured in many models. Furthermore, most models and analytical approaches rely on assumptions to

reduce the dimensionality of the problem. Here, the method and theory are suitable for use on 2-D and three dimensional (3-D) domains and are easily combined with additional energy effects.

2. Energy Model

To begin defining the full energy model under consideration, we first discuss the free elastic energy model. At equilibrium, absent any external forces, fields, or boundary conditions, the free elastic energy present in a liquid crystal sample is given by an integral functional, which depends on the state variables of the system. A liquid crystal sample tends to the state of lowest free energy. While a number of free energy models exist [10], this paper considers the Frank-Oseen free elastic model [27,28]. These equations represent the free elastic energy density, w_F, in a sample as

$$w_F = \frac{1}{2}K_1(\nabla \cdot \mathbf{n})^2 + \frac{1}{2}K_2(\mathbf{n} \cdot \nabla \times \mathbf{n})^2 + \frac{1}{2}K_3|\mathbf{n} \times \nabla \times \mathbf{n}|^2 + \frac{1}{2}(K_2 + K_4)\nabla \cdot [(\mathbf{n} \cdot \nabla)\mathbf{n} - (\nabla \cdot \mathbf{n})\mathbf{n}]. \quad (2.1)$$

Throughout this paper the standard Euclidean inner product and norm are denoted $(\cdot, \cdot)$ and $|\cdot|$, respectively. The K_i, $i = 1, 2, 3, 4$, are known as the Frank elastic constants [15], which vary depending on temperature and liquid crystal type. Let

$$\mathbf{Z} = \kappa \mathbf{n} \otimes \mathbf{n} + (\mathbf{I} - \mathbf{n} \otimes \mathbf{n}) = \mathbf{I} - (1 - \kappa)\mathbf{n} \otimes \mathbf{n},$$

where $\kappa = K_2/K_3$ with $K_2, K_3 \geq 0$ by Ericksen's inequalities [13]. In general, we consider the case that $K_2, K_3 \neq 0$. Denote the classical $L^2(\Omega)$ inner product and norm as $\langle \cdot, \cdot \rangle_0$ and $\| \cdot \|_0$, respectively. Using algebraic identities, the fact that $\mathbf{n}$ has unit length, and integrating the above density function, the total free elastic energy for a domain Ω is

$$\begin{aligned}\int_\Omega w_F \, dV =& \frac{1}{2}(K_1 - K_2 - K_4)\|\nabla \cdot \mathbf{n}\|_0^2 + \frac{1}{2}K_3\langle \mathbf{Z}\nabla \times \mathbf{n}, \nabla \times \mathbf{n}\rangle_0 \\ &+ \frac{1}{2}(K_2 + K_4)\big(\langle \nabla n_1, \frac{\partial \mathbf{n}}{\partial x}\rangle_0 + \langle \nabla n_2, \frac{\partial \mathbf{n}}{\partial y}\rangle_0 + \langle \nabla n_3, \frac{\partial \mathbf{n}}{\partial z}\rangle_0\big).\end{aligned}$$

A number of methods involving computation of liquid crystal equilibria or dynamics utilize the so called one-constant approximation that $K_1 = K_2 = K_3$ and $K_4 = 0$ [8, 24, 27, 29], in order to significantly simplify the free elastic energy density to

$$\hat{w}_F = \frac{1}{2}K_1|\nabla \mathbf{n}|^2, \text{ where } |\nabla \mathbf{n}|^2 = \sum_{i,j}^{3} \left(\frac{\partial n_i}{\partial x_j}\right)^2.$$

This expression for the free elastic energy density is more amenable to theoretical development but ignores significant physical characteristics [3, 19]. The following method is derived without such an assumption.

In the presence of an electric field, the free energy in a liquid crystal sample is directly affected. This interaction is strongly coupled as nematic polarization and electric displacement, in turn, affect the original electric field. The coupling is captured by an auxiliary term added to the Frank-Oseen equations such that the total system free energy has the form

$$\int_\Omega w_F - \frac{1}{2}\mathbf{D} \cdot \mathbf{E} \, dV, \quad (2.2)$$

where $\mathbf{D}$ is the electric displacement vector induced by polarization and $\mathbf{E}$ is the local electric field [11]. The electric displacement vector is written $\mathbf{D} = \epsilon_0\epsilon_\perp \mathbf{E} + \epsilon_0\epsilon_a(\mathbf{n} \cdot \mathbf{E})\mathbf{n}$. Here, $\epsilon_0 > 0$ is the permittivity of free space constant. The dielectric anisotropy constant is $\epsilon_a = \epsilon_\parallel - \epsilon_\perp$, where the constant variables $\epsilon_\parallel > 0$ and $\epsilon_\perp > 0$ represent the parallel and perpendicular dielectric permittivity, respectively, specific to the liquid crystal. If $\epsilon_a > 0$, the director is attracted to parallel alignment with the electric field, and if $\epsilon_a < 0$, the director tends to align perpendicular to $\mathbf{E}$. Thus,

$$\mathbf{D} \cdot \mathbf{E} = \epsilon_0\epsilon_\perp \mathbf{E} \cdot \mathbf{E} + \epsilon_0\epsilon_a(\mathbf{n} \cdot \mathbf{E})^2.$$

Therefore, Equation (2.2) is expanded as

$$\int_\Omega \left(w_F - \frac{1}{2}\mathbf{D} \cdot \mathbf{E}\right) dV = \int_\Omega w_F \, dV - \frac{1}{2}\epsilon_0\epsilon_\perp\langle \mathbf{E}, \mathbf{E}\rangle_0 - \frac{1}{2}\epsilon_0\epsilon_a\langle \mathbf{n} \cdot \mathbf{E}, \mathbf{n} \cdot \mathbf{E}\rangle_0. \quad (2.3)$$

The addition of the electric field not only increases the complexity of the functional, it introduces an inherent saddle-point structure into the equilibria for the liquid crystal samples. Energy minima are those that minimize the contribution of the free elastic energy, while maximizing the negative contribution of the electric field terms. Moreover, the relevant Maxwell's equations for a static electric field, $\nabla \cdot \mathbf{D} = 0$ and $\nabla \times \mathbf{E} = \mathbf{0}$, known as Gauss' and Faraday's laws, respectively, must be satisfied.

3. Free Energy Minimization

In this section, a general approach for computing the equilibrium state for $\mathbf{n}$ is derived. This equilibrium state corresponds to the configuration which minimizes the system free energy subject to the local constraint that $\mathbf{n}$ is of unit length throughout the sample volume, Ω. That is, the minimizer must satisfy $\mathbf{n} \cdot \mathbf{n} = 1$ pointwise throughout the volume. In light of the necessary Maxwell equations, we reformulate the system energy in (2.3) using an electric potential function, ϕ, such that $\mathbf{E} = -\nabla\phi$, and define the functional to be minimized as

$$\begin{aligned}\mathcal{F}_1(\mathbf{n}, \phi) =& (K_1 - K_2 - K_4)\|\nabla \cdot \mathbf{n}\|_0^2 + K_3\langle \mathbf{Z}\nabla \times \mathbf{n}, \nabla \times \mathbf{n}\rangle_0 + (K_2 + K_4)\big(\langle \nabla n_1, \frac{\partial \mathbf{n}}{\partial x}\rangle_0 \\ &+ \langle \nabla n_2, \frac{\partial \mathbf{n}}{\partial y}\rangle_0 + \langle \nabla n_3, \frac{\partial \mathbf{n}}{\partial z}\rangle_0\big) - \epsilon_0\epsilon_\perp\langle \nabla\phi, \nabla\phi\rangle_0 - \epsilon_0\epsilon_a\langle \mathbf{n} \cdot \nabla\phi, \mathbf{n} \cdot \nabla\phi\rangle_0. \end{aligned} \tag{3.1}$$

Using a potential function guarantees that Faraday's law is trivially satisfied. Furthermore, it is not difficult to show that Gauss' law is satisfied at the minimum of the above functional.

For the special case of full Dirichlet boundary conditions, we consider a fixed director $\mathbf{n}$ at each point on the boundary of Ω. Considering the integration carried out for the $(K_2 + K_4)$ term in (2.1), note that since $\mathbf{n}$ is continuously differentiable in Ω,

$$\frac{1}{2}(K_2 + K_4)\int_\Omega \nabla \cdot [(\mathbf{n} \cdot \nabla)\mathbf{n} - (\nabla \cdot \mathbf{n})\mathbf{n}]\, dV = \frac{1}{2}(K_2 + K_4)\int_{\partial\Omega} [(\mathbf{n} \cdot \nabla)\mathbf{n} - (\nabla \cdot \mathbf{n})\mathbf{n}] \cdot \nu\, dS,$$

by the divergence theorem, where ν is the outward unit normal for $\partial\Omega$. Further, since $\mathbf{n}$ is fixed along $\partial\Omega$, the energy contributed by $\mathbf{n}$ on the boundary is constant regardless of the configuration of $\mathbf{n}$ on the interior of Ω. Thus, in the minimization, the energy contribution from this term is ignored and is often referred to as a null Lagrangian [28]. This observation significantly simplifies the functional to be minimized as

$$\mathcal{F}_2(\mathbf{n}, \phi) = K_1\|\nabla \cdot \mathbf{n}\|_0^2 + K_3\langle \mathbf{Z}\nabla \times \mathbf{n}, \nabla \times \mathbf{n}\rangle_0 - \epsilon_0\epsilon_\perp\langle \nabla\phi, \nabla\phi\rangle_0 - \epsilon_0\epsilon_a\langle \mathbf{n} \cdot \nabla\phi, \mathbf{n} \cdot \nabla\phi\rangle_0. \tag{3.2}$$

Note that this simplification is also applicable to a rectangular domain with mixed Dirichlet and periodic boundary conditions. Such a domain is considered in the numerical experiments presented here.

We proceed with the functional in (3.1) in building a framework for minimization under general boundary conditions. However, in the treatment of existence and uniqueness theory, we assume the presence of full Dirichlet boundary conditions and, therefore, apply the simplification in (3.2).

Next, we consider the spaces

$$H(\mathrm{div}, \Omega) = \{\mathbf{v} \in L^2(\Omega)^3 : \nabla \cdot \mathbf{v} \in L^2(\Omega)\}, \qquad H(\mathrm{curl}, \Omega) = \{\mathbf{v} \in L^2(\Omega)^3 : \nabla \times \mathbf{v} \in L^2(\Omega)^3\}.$$

Define

$$\mathcal{H}^{DC}(\Omega) = \{\mathbf{v} \in H(\mathrm{div}, \Omega) \cap H(\mathrm{curl}, \Omega) : B(\mathbf{v}) = \bar{g}\},$$

with norm $\|\mathbf{v}\|_{DC}^2 = \|\mathbf{v}\|_0^2 + \|\nabla \cdot \mathbf{v}\|_0^2 + \|\nabla \times \mathbf{v}\|_0^2$ and appropriate boundary conditions $B(\mathbf{v}) = \bar{g}$. Further, let $\mathcal{H}_0^{DC}(\Omega) = \{\mathbf{v} \in H(\mathrm{div}, \Omega) \cap H(\mathrm{curl}, \Omega) : B(\mathbf{v}) = \mathbf{0}\}$. Let

$$H^{1,g}(\Omega) = \{f \in H^1(\Omega) : B_1(f) = g\},$$

where $H^1(\Omega)$ represents the classical Sobolev space and $B_1(f)$ is an appropriate boundary condition expression. Finally, denote the unit sphere as $\mathcal{S}^2$. Using Functional (3.1), the desired minimization becomes

$$(\mathbf{n}_0, \phi_0) = \underset{(\mathbf{n},\phi)\in(\mathcal{S}^2\cap\mathcal{H}^{DC}(\Omega))\times H^{1,g}(\Omega)}{\mathrm{argmin}} \mathcal{F}_1(\mathbf{n}, \phi).$$

3.1. **First-Order Continuum Optimality Conditions.** Since $\mathbf{n}$ must be of unit length, it is natural to employ a Lagrange multiplier approach. This length requirement represents a pointwise equality constraint such that $(\mathbf{n},\mathbf{n})-1=0$. Thus, following general constrained optimization theory [22], define the Lagrangian

$$\mathcal{L}(\mathbf{n},\phi,\lambda)=\mathcal{F}_1(\mathbf{n},\phi)+\int_\Omega \lambda(\mathbf{x})((\mathbf{n},\mathbf{n})-1)\,dV,$$

where $\lambda\in L^2(\Omega)$. In order to minimize (3.1), we compute the Gâteaux derivatives of $\mathcal{L}$ with respect to $\mathbf{n}$, ϕ, and λ in the directions $\mathbf{v}\in\mathcal{H}_0^{DC}(\Omega)$, $\psi\in H^{1,0}(\Omega)$, and $\gamma\in L^2(\Omega)$, respectively. Hence, necessary continuum first-order optimality conditions are derived as

$$\begin{aligned}
\mathcal{L}_{\mathbf{n}}[\mathbf{v}] &= \frac{\partial}{\partial \mathbf{n}}\mathcal{L}(\mathbf{n},\phi,\lambda)[\mathbf{v}]=0, && \forall \mathbf{v}\in\mathcal{H}_0^{DC}(\Omega),\\
\mathcal{L}_{\phi}[\psi] &= \frac{\partial}{\partial \phi}\mathcal{L}(\mathbf{n},\phi,\lambda)[\psi]=0, && \forall \psi\in H^{1,0}(\Omega),\\
\mathcal{L}_{\lambda}[\gamma] &= \frac{\partial}{\partial \lambda}\mathcal{L}(\mathbf{n},\phi,\lambda)[\gamma]=0, && \forall \gamma\in L^2(\Omega).
\end{aligned}$$

Computing these derivatives yields the variational system

$$\begin{aligned}
\mathcal{L}_{\mathbf{n}}[\mathbf{v}] =& 2(K_1-K_2-K_4)\langle\nabla\cdot\mathbf{n},\nabla\cdot\mathbf{v}\rangle_0+2K_3\langle\mathbf{Z}\nabla\times\mathbf{n},\nabla\times\mathbf{v}\rangle_0\\
&+2(K_2-K_3)\langle\mathbf{n}\cdot\nabla\times\mathbf{n},\mathbf{v}\cdot\nabla\times\mathbf{n}\rangle_0+2(K_2+K_4)\big(\langle\nabla n_1,\frac{\partial\mathbf{v}}{\partial x}\rangle_0+\langle\nabla n_2,\frac{\partial\mathbf{v}}{\partial y}\rangle_0\\
&+\langle\nabla n_3,\frac{\partial\mathbf{v}}{\partial z}\rangle_0\big)-2\epsilon_0\epsilon_a\langle\mathbf{n}\cdot\nabla\phi,\mathbf{v}\cdot\nabla\phi\rangle_0+2\int_\Omega\lambda(\mathbf{n},\mathbf{v})\,dV=0, && \forall\mathbf{v}\in\mathcal{H}_0^{DC}(\Omega),\\
\mathcal{L}_{\phi}[\psi] =& -2\epsilon_0\epsilon_\perp\langle\nabla\phi,\nabla\psi\rangle_0-2\epsilon_0\epsilon_a\langle\mathbf{n}\cdot\nabla\phi,\mathbf{n}\cdot\nabla\psi\rangle_0=0, && \forall\psi\in H^{1,0}(\Omega),\\
\mathcal{L}_{\lambda}[\gamma] =& \int_\Omega\gamma((\mathbf{n},\mathbf{n})-1)\,dV=0, && \forall\gamma\in L^2(\Omega).
\end{aligned}$$

3.2. **Nonlinearities and Newton Linearization.** The system above is nonlinear; therefore, Newton iterations are employed by computing a generalized first-order Taylor series expansion, requiring computation of the Hessian. Let $\mathbf{n}_k$, ϕ_k, and λ_k be the current approximations for $\mathbf{n}$, ϕ, and λ, respectively. Additionally, let $\delta\mathbf{n}=\mathbf{n}_{k+1}-\mathbf{n}_k$, $\delta\phi=\phi_{k+1}-\phi_k$, and $\delta\lambda=\lambda_{k+1}-\lambda_k$ be updates to the current approximations that we seek to compute. Then, the Newton iterations are denoted

$$\begin{bmatrix}\mathcal{L}_{\mathbf{nn}} & \mathcal{L}_{\mathbf{n}\phi} & \mathcal{L}_{\mathbf{n}\lambda}\\ \mathcal{L}_{\phi\mathbf{n}} & \mathcal{L}_{\phi\phi} & \mathcal{L}_{\phi\lambda}\\ \mathcal{L}_{\lambda\mathbf{n}} & \mathcal{L}_{\lambda\phi} & \mathcal{L}_{\lambda\lambda}\end{bmatrix}\begin{bmatrix}\delta\mathbf{n}\\ \delta\phi\\ \delta\lambda\end{bmatrix}=-\begin{bmatrix}\mathcal{L}_{\mathbf{n}}\\ \mathcal{L}_{\phi}\\ \mathcal{L}_{\lambda}\end{bmatrix},\tag{3.3}$$

where each of the system components are evaluated at $\mathbf{n}_k$, ϕ_k, and λ_k. The matrix-vector multiplication indicates the direction that the derivatives in the Hessian are taken. For instance,

$$\mathcal{L}_{\lambda\mathbf{n}}[\gamma]\cdot\delta\mathbf{n}=\frac{\partial}{\partial\mathbf{n}}\left(\mathcal{L}_\lambda(\mathbf{n}_k,\lambda_k)[\gamma]\right)[\delta\mathbf{n}],$$

where the partials indicate Gâteaux derivatives in the respective variables. Note that $\mathcal{L}_{\lambda\lambda}=\mathcal{L}_{\lambda\phi}=\mathcal{L}_{\phi\lambda}=0$. Hence, the Hessian in (3.3) simplifies to the saddle-point structure,

$$\begin{bmatrix}\mathcal{L}_{\mathbf{nn}} & \mathcal{L}_{\mathbf{n}\phi} & \mathcal{L}_{\mathbf{n}\lambda}\\ \mathcal{L}_{\phi\mathbf{n}} & \mathcal{L}_{\phi\phi} & \mathbf{0}\\ \mathcal{L}_{\lambda\mathbf{n}} & \mathbf{0} & \mathbf{0}\end{bmatrix}.\tag{3.4}$$

The discrete form of this Hessian leads to a saddle-point matrix, which poses unique difficulties for the efficient computation of the solution to the resulting linear system. Such structures commonly appear in constrained optimization and other settings; for a comprehensive overview of discrete saddle-point problems see [6]. Here, we focus only on the linearization step rather than the underlying linear solvers. Considering the other six components of the Hessian, the derivatives involving λ are

$$\mathcal{L}_{\lambda\mathbf{n}}[\gamma]\cdot\delta\mathbf{n}=2\int_\Omega\gamma(\mathbf{n}_k,\delta\mathbf{n})\,dV,\qquad\qquad\mathcal{L}_{\mathbf{n}\lambda}[\mathbf{v}]\cdot\delta\lambda=2\int_\Omega\delta\lambda(\mathbf{n}_k,\mathbf{v})\,dV.$$

The second order terms involving ϕ are

$$\begin{aligned}
\mathcal{L}_{\phi\phi}[\psi]\cdot\delta\phi &= -2\epsilon_0\epsilon_\perp\langle\nabla\delta\phi,\nabla\psi\rangle_0 - 2\epsilon_0\epsilon_a\langle\mathbf{n}_k\cdot\nabla\delta\phi,\mathbf{n}_k\cdot\nabla\psi\rangle_0,\\
\mathcal{L}_{\phi\mathbf{n}}[\psi]\cdot\delta\mathbf{n} &= -2\epsilon_0\epsilon_a\langle\mathbf{n}_k\cdot\nabla\phi_k,\delta\mathbf{n}\cdot\nabla\psi\rangle_0 - 2\epsilon_0\epsilon_a\langle\delta\mathbf{n}\cdot\nabla\phi_k,\mathbf{n}_k\cdot\nabla\psi\rangle_0,\\
\mathcal{L}_{\mathbf{n}\phi}[\mathbf{v}]\cdot\delta\phi &= -2\epsilon_0\epsilon_a\langle\mathbf{n}_k\cdot\nabla\phi_k,\mathbf{v}\cdot\nabla\delta\phi\rangle_0 - 2\epsilon_0\epsilon_a\langle\mathbf{n}_k\cdot\nabla\delta\phi,\mathbf{v}\cdot\nabla\phi_k\rangle_0.
\end{aligned}$$

Finally, the second order $\mathbf{n}$ derivative is

$$\begin{aligned}
\mathcal{L}_{\mathbf{nn}}[\mathbf{v}]\cdot\delta\mathbf{n} =& 2(K_1-K_2-K_4)\langle\nabla\cdot\delta\mathbf{n},\nabla\cdot\mathbf{v}\rangle_0 + 2K_3\langle\mathbf{Z}(\mathbf{n}_k)\nabla\times\delta\mathbf{n},\nabla\times\mathbf{v}\rangle_0\\
&+ 2(K_2-K_3)\Big(\langle\delta\mathbf{n}\cdot\nabla\times\mathbf{v},\mathbf{n}_k\cdot\nabla\times\mathbf{n}_k\rangle_0 + \langle\mathbf{n}_k\cdot\nabla\times\mathbf{v},\delta\mathbf{n}\cdot\nabla\times\mathbf{n}_k\rangle_0\\
&+ \langle\mathbf{n}_k\cdot\nabla\times\mathbf{n}_k,\mathbf{v}\cdot\nabla\times\delta\mathbf{n}\rangle_0 + \langle\mathbf{n}_k\cdot\nabla\times\delta\mathbf{n},\mathbf{v}\cdot\nabla\times\mathbf{n}_k\rangle_0\\
&+ \langle\delta\mathbf{n}\cdot\nabla\times\mathbf{n}_k,\mathbf{v}\cdot\nabla\times\mathbf{n}_k\rangle_0\Big) + 2(K_2+K_4)\big(\langle\nabla\delta n_1,\frac{\partial\mathbf{v}}{\partial x}\rangle_0 + \langle\nabla\delta n_2,\frac{\partial\mathbf{v}}{\partial y}\rangle_0\\
&+ \langle\nabla\delta n_3,\frac{\partial\mathbf{v}}{\partial z}\rangle_0\big) - 2\epsilon_0\epsilon_a\langle\delta\mathbf{n}\cdot\nabla\phi_k,\mathbf{v}\cdot\nabla\phi_k\rangle_0 + 2\int_\Omega\lambda_k(\delta\mathbf{n},\mathbf{v})\,dV.
\end{aligned}$$

Completing (3.3) with the above Hessian computations yields a linearized variational system. For these iterations, we compute $\delta\mathbf{n}$, $\delta\phi$, and $\delta\lambda$ satisfying (3.3) for all $\mathbf{v}\in\mathcal{H}_0^{DC}(\Omega)$, $\psi\in H^{1,0}(\Omega)$, and $\gamma\in L^2(\Omega)$ with the current approximations $\mathbf{n}_k$, ϕ_k, and λ_k. While they typically improve robustness and efficiency, we do not consider the use of line searches or trust regions in the work presented here, leaving this for future work. If we are considering a system with Dirichlet boundary conditions, as described above, we eliminate the (K_2+K_4) terms from (3.3). This produces a simplified, but still complicated, linearization.

4. Well-Posedness of the Discrete Systems

Performing the outlined Newton iterations necessitates solving the above linearized systems for the update functions $\delta\mathbf{n}$, $\delta\phi$, and $\delta\lambda$. Finite elements are used to numerically approximate these updates as $\delta\mathbf{n}_h$, $\delta\phi_h$, and $\delta\lambda_h$. Throughout this section, we assume that full Dirichlet boundary conditions are enforced for $\mathbf{n}$ and ϕ. However, the following theory is also applicable for a rectangular domain with mixed Dirichlet and periodic boundary conditions. Such a domain is considered for the numerical experiments presented herein.

We write the bilinear form defined by $-\mathcal{L}_{\phi\phi}[\psi]\cdot\delta\phi$ as $c(\delta\phi,\psi)=\epsilon_0\epsilon_\perp\langle\nabla\delta\phi,\nabla\psi\rangle_0+\epsilon_0\epsilon_a\langle\mathbf{n}_k\cdot\nabla\delta\phi,\mathbf{n}_k\cdot\nabla\psi\rangle_0$ and the form associated with $\mathcal{L}_{\lambda\mathbf{n}}[\gamma]\cdot\delta\mathbf{n}$ as $b(\delta\mathbf{n},\gamma)$. Further, we will decompose the bilinear form defined by $\mathcal{L}_{\mathbf{nn}}[\mathbf{v}]\cdot\delta\mathbf{n}$ into a free elastic term, $\tilde{a}(\delta\mathbf{n},\mathbf{v})$, and an electric component as

$$a(\delta\mathbf{n},\mathbf{v}) = \tilde{a}(\delta\mathbf{n},\mathbf{v}) - \epsilon_0\epsilon_a\langle\delta\mathbf{n}\cdot\nabla\phi_k,\mathbf{v}\cdot\nabla\phi_k\rangle_0.$$

Lemma 4.1. *Let Ω be a connected, open, bounded domain. If $\epsilon_a\geq 0$, then $c(\delta\phi,\psi)$ is a positive-definite bilinear form. For $\epsilon_a<0$, if $|\mathbf{n}_k|^2\leq\beta<\epsilon_\perp/|\epsilon_a|$, for $\beta\geq 1$, then $c(\delta\phi,\psi)$ is a positive-definite bilinear form.*

Proof. The proof is split into two cases.

Case 1. $\epsilon_a\geq 0$.
Note that $\delta\phi,\psi\in H^{1,0}(\Omega)$, with homogeneous Dirichlet boundary conditions. By the classical Poincaré-Friedrichs' inequality, there exists a $C_1>0$ such that for all $\xi\in H_0^1(\Omega)$, $\|\xi\|_0^2\leq C_1\|\nabla\xi\|_0^2$. This implies that, for $\xi\neq 0$,

$$\begin{aligned}
c(\xi,\xi) &= \epsilon_0\epsilon_\perp\langle\nabla\xi,\nabla\xi\rangle_0 + \epsilon_0\epsilon_a\langle\mathbf{n}_k\cdot\nabla\xi,\mathbf{n}_k\cdot\nabla\xi\rangle_0\\
&\geq \frac{\epsilon_0\epsilon_\perp}{C_1}\|\xi\|_0^2 > 0.
\end{aligned}$$

Case 2. $\epsilon_a<0$.
Observe that pointwise,

$$(\mathbf{n}_k\cdot\nabla\xi)^2\leq|\mathbf{n}_k|^2|\nabla\xi|^2\leq\beta|\nabla\xi|^2.$$

This implies that $\langle\mathbf{n}_k\cdot\nabla\xi,\mathbf{n}_k\cdot\nabla\xi\rangle_0\leq\beta\langle\nabla\xi,\nabla\xi\rangle_0$. Therefore,

$$c(\xi,\xi)\geq\epsilon_0(\epsilon_\perp-\beta|\epsilon_a|)\langle\nabla\xi,\nabla\xi\rangle_0.$$

Recall that $\epsilon_\parallel > 0$. Therefore, $\epsilon_\perp/|\epsilon_a| > 1$, and $\beta < \epsilon_\perp/|\epsilon_a|$ implies that $\epsilon_\perp - \beta|\epsilon_a| > 0$. Thus, again applying the Poincaré-Friedrichs' inequality above for $\xi \neq 0$,

$$c(\xi,\xi) \geq \frac{\epsilon_0(\epsilon_\perp + \beta\epsilon_a)}{C_1}\|\xi\|_0^2 > 0.$$

In either case, $c(\cdot,\cdot)$ is a positive-definite bilinear form. □

There are a number of discretization space triples commonly used to discretize systems such as the one defined in (3.3), including equal order or mixed finite elements. Discretizing the Hessian in (3.4) with finite elements leads to the 3×3 block matrix

$$\begin{bmatrix} A & B_1 & B_2 \\ B_1^T & -\tilde{C} & \mathbf{0} \\ B_2^T & \mathbf{0} & \mathbf{0} \end{bmatrix}. \tag{4.1}$$

Lemma 4.2. *Under the assumptions in Lemma 4.1, if the bilinear forms $a(\cdot,\cdot)$ and $b(\cdot,\cdot)$, defined above, are coercive and weakly coercive, respectively, on the relevant discrete spaces, the matrix in* (4.1) *is invertible.*

Proof. Denoting $B = \begin{bmatrix} B_1 & B_2 \end{bmatrix}$ (where B_2 is associated with $b(\cdot,\cdot)$), and $C = \begin{bmatrix} \tilde{C} & \mathbf{0} \\ \mathbf{0} & \mathbf{0} \end{bmatrix}$, the matrix in (4.1) is written as

$$\begin{bmatrix} A & B \\ B^T & -C \end{bmatrix}.$$

By assumption, $a(\cdot,\cdot)$ is coercive, and it is clearly symmetric. Therefore, the associated discretization block, A, is symmetric positive definite. By Lemma (4.1), $\tilde{C}$ is symmetric positive definite, and, therefore, $-C$ is symmetric negative semi-definite. Therefore, by [6, Theorem 3.1], if $\ker C \cap \ker B = \{\mathbf{0}\}$, then the matrix in (4.1) is invertible. Observe that

$$\begin{bmatrix} \tilde{C} & \mathbf{0} \\ \mathbf{0} & \mathbf{0} \end{bmatrix}\begin{bmatrix} \mathbf{y} \\ \mathbf{z} \end{bmatrix} = \begin{bmatrix} \tilde{C}\mathbf{y} \\ \mathbf{0} \end{bmatrix} = \mathbf{0}$$

if and only if $\mathbf{y} = \mathbf{0}$. Then, if $\begin{bmatrix} \mathbf{y} & \mathbf{z} \end{bmatrix}^T \in \ker C \cap \ker B$, $\mathbf{y} = \mathbf{0}$. However, note that

$$\begin{bmatrix} B_1 & B_2 \end{bmatrix}\begin{bmatrix} \mathbf{0} \\ \mathbf{z} \end{bmatrix} = B_2\mathbf{z}.$$

Since $b(\cdot,\cdot)$ is weakly coercive, $B_2\mathbf{z} = \mathbf{0}$ if and only if $\mathbf{z} = \mathbf{0}$. So $\ker C \cap \ker B = \{\mathbf{0}\}$. □

We have shown in [1] that the assumptions of Lemma 4.2 are satisfied under reasonable conditions. In particular, it is sufficient that Ω be a polygonal domain subject to a quasi-uniform quadrilateral subdivision and that $|\mathbf{n}_k|^2$ be appropriately bounded above and below. Additionally, it is required that we are close enough to the solution that λ_k is pointwise non-negative and that $\kappa = 1$ or satisfies the small data assumption in [1, Lemma 3.8]. If the discrete space for $\delta\lambda$ is piecewise constants, P_0, and the discrete space for $\delta\mathbf{n}$ is the space of piecewise C^0 polynomials of degree $p \geq 1$, Q_p, enriched with proper bubble functions, then $\tilde{a}(\cdot,\cdot)$ is coercive and $b(\cdot,\cdot)$ is weakly coercive [1]. Thus, $a(\cdot,\cdot)$ is coercive as long as $\epsilon_a < 0$ or the magnitude of $\nabla\phi_k$ is not too large. Therefore, Lemma 4.2 implies that no additional inf-sup condition for ϕ is necessary to guarantee uniqueness of the solution to the system in (3.3), and the discretization space for ϕ may be freely chosen without concern for stability.

5. Numerical Methodology

The algorithm to perform the minimization discussed in previous sections has three stages; see Algorithm 1. The outermost phase is nested iteration (NI) [23, 26], which begins on a specified coarsest grid level. Newton iterations are performed on each grid, updating the current approximation after each step. The stopping criterion for the Newton iterations at each level is based on a specified tolerance for the current approximation's conformance to the first-order optimality conditions in the standard Euclidean l_2 norm. The resulting approximation is then interpolated to a finer grid. The current implementation performs uniform grid refinement after each set of Newton iterations.

The linear system for each Newton step has the anticipated saddle-point block structure, detailed in (4.1). The matrix is inverted using LU decomposition in order to solve for the discrete updates $\delta\mathbf{n}_h$, $\delta\phi_h$, and $\delta\lambda_h$. Finally, an incomplete Newton correction is performed. That is, the new iterates are given by

$$\begin{bmatrix} \mathbf{n}_{k+1} \\ \phi_{k+1} \\ \lambda_{k+1} \end{bmatrix} = \begin{bmatrix} \mathbf{n}_k \\ \phi_k \\ \lambda_k \end{bmatrix} + \omega \begin{bmatrix} \delta\mathbf{n}_h \\ \delta\phi_h \\ \delta\lambda_h \end{bmatrix}, \tag{5.1}$$

where $\omega \leq 1$. This is to ensure relatively strict adherence to the constraint manifold, which is necessary for the invertibility discussed above. For this algorithm, ω is chosen to begin at 0.2 on the coarsest grid and increases by 0.2, to a maximum of 1, after each grid refinement, so that as the approximation converges, larger Newton steps are taken. The grid management and discretizations are implemented using the deal.II finite-element library, which is an aggressively optimized and parallelized open-source library widely used in scientific computing [4, 5]. In practice, Q_2–Q_2–P_0 discretizations were observed to experimentally admit unique solutions and were used to approximate $\delta\mathbf{n}_h$, $\delta\phi_h$, and $\delta\lambda_h$, respectively, on each grid for the following numerical tests.

Algorithm 1: Newton's method minimization algorithm with NI

0. Initialize $(\mathbf{n}_0, \phi_0, \lambda_0)$ on coarse grid.
while *Refinement limit not reached* **do**
  while *First-order optimality conformance threshold not satisfied* **do**
    1. Set up discrete linear system (3.3) on current grid, H.
    2. Solve for $\delta\mathbf{n}_H$, $\delta\phi_H$, and $\delta\lambda_H$.
    3. Compute $\mathbf{n}_{k+1}$, ϕ_{k+1}, and λ_{k+1} as in (5.1).
  end
  4. Uniformly refine the grid.
  5. Interpolate $\mathbf{n}_H \to \mathbf{n}_h$, $\phi_H \to \phi_h$, and $\lambda_H \to \lambda_h$.
end

5.1. **Freedericksz Transition Results.** The general test problem in this section considers a classical domain with two parallel substrates placed at distance $d = 1$ apart. The substrates run parallel to the xz-plane and perpendicular to the y-axis. It is assumed that this domain represents a uniform slab in the xy-plane. That is, $\mathbf{n}$ may have a non-zero z component but $\frac{\partial \mathbf{n}}{\partial z} = \mathbf{0}$. Hence, we consider the 2-D domain $\Omega = \{(x, y) \mid 0 \leq x, y \leq 1\}$. The problem assumes periodic boundary conditions at the edges $x = 0$ and $x = 1$. Dirichlet boundary conditions are enforced on the y-boundaries. As discussed above, the simplification outlined in (3.2) is relevant for this domain and boundary conditions.

The first numerical experiment considers simple director boundary conditions, such that $\mathbf{n}$, along both of the substrates, lies uniformly parallel to the x-axis. The boundary conditions for the electric potential, ϕ, are such that $\phi = 0$ on the lower substrate at $y = 0$ and $\phi = 1$ at $y = 1$. The relevant constants for the problem are detailed in Table 1. Since the electric anisotropy constant, ϵ_a, is positive, the expected behavior for the liquid crystal configuration is a Freedericksz transition [16,30] so long as the applied field is strong enough to overcome the inherent elastic effects of the system. That is, for an applied voltage above a critical threshold, known as a Freedericksz threshold [27], the liquid crystal configuration will depart from uniform alignment parallel to the x-axis and instead tilt in the direction of the applied field. The problem considered has an analytical solution [27, pg. 92-93] demonstrating this behavior. The critical voltage is given by $V_c = \pi\sqrt{\frac{K_1}{\epsilon_0\epsilon_a}}$. For the constants detailed in Table 1, this implies a Freedericksz threshold of 0.7752. Thus, the anticipated solution should demonstrate a true Freedericksz transition away from uniform free elastic alignment. Indeed, the final computed solution in Figure 1, displayed alongside the initial guess for the algorithm, displays the expected transition.

The problem is solved on a 4×4 coarse grid with seven successive uniform refinements resulting in a 512×512 fine grid. The minimized functional energy is $\mathcal{F}_2 = -5.330$, compared to the initial guess energy of 7.416. Figure 2 details the number of Newton iterations necessary to reduce the residual below the given tolerance, 10^{-3}, on each grid. Note that a sizable majority of the Newton iteration computations are isolated

Elastic Constants	$K_1 = 1$	$K_2 = 0.62903$	$K_3 = 1.32258$	$\kappa = 0.475608$
Electric Constants	$\epsilon_0 = 1.42809$	$\epsilon_{\|} = 18.5$	$\epsilon_{\perp} = 7$	$\epsilon_a = 11.5$

TABLE 1. Relevant liquid crystal constants for Freedericksz transition problem.

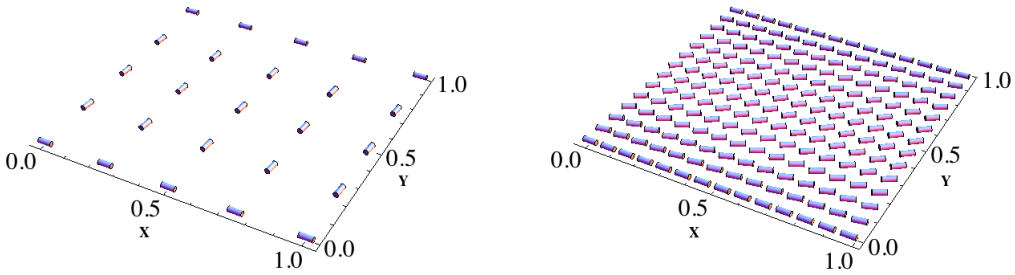

FIGURE 1. Initial guess (left) on 4×4 mesh with initial free energy of 7.416 and resolved solution (right) on 512×512 mesh (restricted for visualization) with final free energy of -5.330 for Freedericksz transition.

to the coarsest grids, with the finest grids requiring only one Newton iteration to reach the tolerance limit. Assuming the presence of solvers that scale linearly with the number of non-zeros in the matrix, the work required in these iterations is roughly 1.43 times that of assembling and solving a single linearization step on the finest grid. Without the use of nested iteration, the algorithm requires 78 Newton steps on the finest grid, alone, to reach a similar error measure.

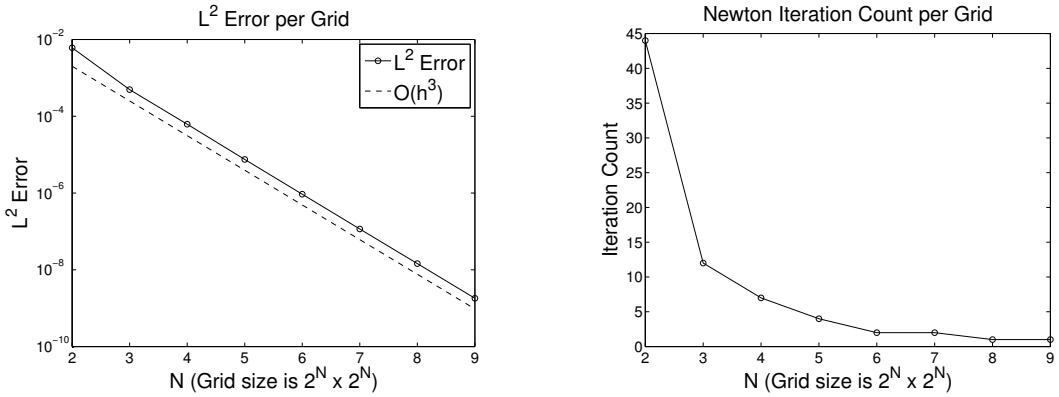

FIGURE 2. L^2 error (left) and Newton iterations (right) per grid for the Freedericksz transition.

Also detailed in Figure 2 is the reduction in overall L^2-error comparing the analytical solution to the resolved solution on each grid. Note that the error is approximately reduced by a full order of magnitude on each successive grid, corresponding to approximately order h^3 reductions in overall error. Moreover, for the finer grids, a single Newton step was sufficient to achieve such a reduction.

5.2. **Electric Field with Patterned Boundary Conditions Results.** In the second run, more complicated boundary conditions are considered. Letting $r = 0.25$ and $s = 0.95$, the boundary conditions considered were

$$\mathbf{n} = \left(0, \cos\left(r(\pi + 2\tan^{-1}(X_m) - 2\tan^{-1}(X_p))\right), \sin\left(r(\pi + 2\tan^{-1}(X_m) - 2\tan^{-1}(X_p))\right)\right),$$

where $X_m = \frac{-s\sin(2\pi(x+r))}{-s\cos(2\pi(x+r))-1}$ and $X_p = \frac{-s\sin(2\pi(x+r))}{-s\cos(2\pi(x+r))+1}$. Such boundary conditions are meant to simulate nano-patterned surfaces important in current research [2,3]; see the substrate boundaries in Figure 3. Even in the absence of electric fields, such patterned surfaces result in complicated director configurations throughout the interior of Ω.

The same constants outlined in Table 1 are used for this problem. However, a stronger voltage such that $\phi = 2$ on the substrate at $y = 1$ is applied. Along the other substrate, ϕ remains equal to 0. The final solution, as well as the initial guess, are displayed in Figure 3. For this problem, the grid progression begins on a 4×4 grid with five successive uniform refinements ascending to a 128×128 fine grid. The minimized functional energy is $\mathcal{F}_2 = -41.960$, compared to the initial guess energy of -40.731. In Table 2, the number of Newton iterations per grid is detailed as well as the conformance of the solution to the first-order optimality conditions after the first and final Newton steps, respectively, on each grid. As with the previous example, much of the computational work is relegated to the coarsest grids. Here, the total work required is approximately 3.35 times that of assembling and solving a single linearization step on the finest grid. In contrast, without nested iteration, the algorithm requires 49 Newton steps on the 128×128 fine grid, alone, to satisfy the tolerance limit. The average length of the director for the resolved solution exactly conforms to the unit length constraint.

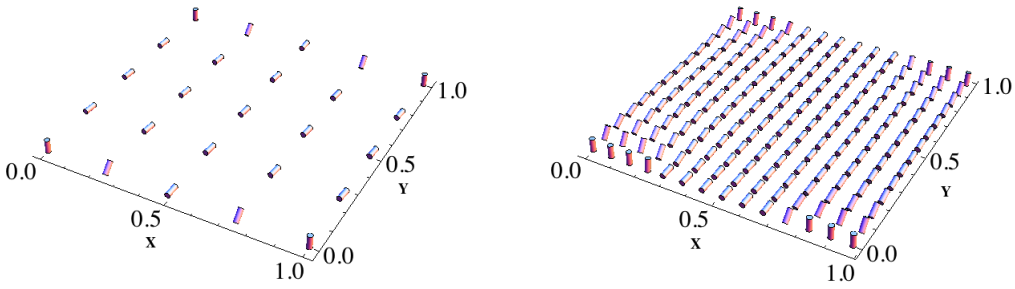

FIGURE 3. Initial guess (left) on 4×4 mesh with initial free energy of -40.731 and resolved solution (right) on 128×128 mesh (restricted for visualization) with final free energy of -41.960 for nano-patterned boundary.

Grid Dimensions	Newton iterations	Initial Residual	Final Residual	Avg. $\lvert\mathbf{n}\rvert^2$
4×4	44	1.44e+01	9.86e-04	1
8×8	18	5.46e-00	9.44e-04	1
16×16	10	2.01e-00	5.41e-04	1
32×32	6	9.91e-01	3.17e-04	1
64×64	3	5.52e-01	3.14e-07	1
128×128	2	2.36e-01	1.36e-04	1

TABLE 2. Grid and solution progression for electric problem with nano-patterned boundary.

Due to the sizable applied electric field, and the elastic influence of the central boundary condition pattern aligned with the electric field, the expected configuration is a quick transition from the boundary conditions to uniform alignment with the field. That is, the strength of the Freedericksz transition on the interior of Ω is augmented by the presence of this type of patterned boundary condition. This behavior is accurately resolved in the computed solution.

6. Summary and Future Work

We have discussed a constrained minimization approach to solving for liquid crystal equilibrium configurations in the presence of applied electric fields. Such minimization is founded upon the electrically augmented Frank-Oseen model. Due to the nonlinearity of the continuum first-order optimality conditions, Newton linearizations were needed. The discrete Hessian arising in the finite-element discretization of these linearized systems was shown to be invertible under certain assumptions on the bilinear forms. Using the finite-element spaces discussed in [1], these assumptions are satisfied. Future work will include developing tailored solvers for these systems.

Numerical results demonstrated the accuracy and efficiency of the algorithm in resolving both classical and complicated features induced by applied fields. The minimization approach overcomes some difficulties inherent to the liquid crystal equilibrium problem, such as the nonlinear unit length director constraint

and effectively deals with heterogeneous Frank constants. The algorithm also productively utilizes nested iterations to reduce computational costs by isolating much of the computational work to the coarsest grids. The above method is currently being extended to include flexoelectric effects in order to more accurately capture physical phenomenon important to many applications, such as the study of bistable devices [9]. Future work will also include the study of effective adaptive refinement and linearization tolerance schemes.

Acknowledgments

The authors would like to thank Professor Thomas Manteuffel for his useful contributions and suggestions.

References

[1] J.H. Adler, T.J. Atherton, D.B. Emerson, and S.P. MacLachlan. An energy-minimization finite-element approach for the Frank-Oseen model of nematic liquid crystals. *In Preparation*, 2014.

[2] T.J. Atherton and J.H. Adler. Competition of elasticity and flexoelectricity for bistable alignment of nematic liquid crystals on patterned surfaces. *Phys. Rev. E*, 86, 2012.

[3] T.J. Atherton and J.R. Sambles. Orientational transition in a nematic liquid crystal at a patterned surface. *Phys. Rev. E*, 74, 2006.

[4] W. Bangerth, R. Hartmann, and G. Kanschat. deal.II – a general purpose object oriented finite element library. *ACM Trans. Math. Softw.*, 33(4):24/1–24/27, 2007.

[5] W. Bangerth, T. Heister, G. Kanschat, et al. `deal.II` *Differential Equations Analysis Library, Technical Reference.* `http://www.dealii.org`.

[6] M. Benzi, G. H. Golub, and J. Liesen. Numerical solution of saddle point problems. *Acta Numerica*, pages 1–137, 2005.

[7] S. Chandrasekhar. *Liquid Crystals*. Cambridge University Press, Cambridge, 2nd edition, 1992.

[8] R. Cohen, R. Hardt, D. Kinderlehrer, S. Lin, and M. Luskin. Minimum energy configurations for liquid crystals: Computational results. In *Theory and Applications of Liquid Crystals*, volume 5 of *The IMA Volumes in Mathematics and Its Applications*, pages 99–121. Springer-Verlag, 1987.

[9] A.J. Davidson and N.J. Mottram. Flexoelectric switching in a bistable nematic device. *Phys. Rev. E*, 65(5), May 2002.

[10] T.A. Davis and E.C. Gartland Jr. Finite element analysis of the Landau-de Gennes minimization problem for liquid crystals. *SIAM J. Numer. Anal.*, 1:336–362, 1998.

[11] P.G. de Gennes and J. Prost. *The Physics of Liquid Crystals*. Clarendon Press, Oxford, 2nd edition, 1993.

[12] J.L. Ericksen. Hydrostatic theory of liquid crystals. *Arch. Rat. Mech. Anal.*, 9:371–378, 1962.

[13] J.L. Ericksen. Inequalities in liquid crystal theory. *Phys. Fluids*, 9:1205–1207, 1966.

[14] L.P. Franca and S.L. Frey. Stabilized finite element methods: II. the incompressible Navier-Stokes equations. *Comput. Methods Appl. Mech. Engrg.*, 99:209–233, 1992.

[15] F.C. Frank. On the theory of liquid crystals. *Discuss. Faraday Soc.*, 25:19–28, 1958.

[16] V. Freedericksz and V. Zolina. Forces causing the orientation of an anisotropic liquid. *Trans. Faraday Soc.*, 29:919–930, 1933.

[17] E.C. Gartland Jr. and A. Ramage. Local stability and a renormalized Newton method for equilibrium liquid crystal director modeling. Working paper, University of Strathclyde, 2012.

[18] J.P.F. Lagerwall and G. Scalia. A new era for liquid crystal research: Applications of liquid crystals in soft matter, nano-, bio- and microtechnology. *Current Applied Physics*, pages 1–26, 2012.

[19] B.W. Lee and N.A. Clark. Alignment of liquid crystals with patterned isotropic surfaces. *Science*, 291(5513):2576–2580, March 2001.

[20] C. Liu and H. Sun. On energetic variational approaches in modeling the nematic liquid crystal flows. *Discrete Contin. Dyn. Syst.*, 23(2):455–475, 2009.

[21] C. Liu, H. Zhang, and S. Zhang. Numerical simulations of hydrodynamics of nematic liquid crystals: Effects of kinematic transports. *Phys. Rev. E*, 9(4):974–993, 2010.

[22] D.G. Luenberger. *Optimization by Vector Space Methods*. John Wiley and Sons, Inc., New York, 1969.

[23] S. McCormick. A mesh refinement method for $Ax = \lambda Bx$. *Math. Comp.*, 36(154):485–498, 1981.

[24] A. Ramage and E.C. Gartland Jr. A preconditioned nullspace method for liquid crystal director modeling. *SIAM J. Sci. Comput.*, 35(1):B226–B247, 2013.

[25] F. Reinitzer. Beitrage zur kenntnis des cholesterins. *Monatsh. Chem.*, 9:421–441, 1888.

[26] G. Starke. Gauss-Newton multilevel methods for least-squares finite element computations of variably saturated subsurface flow. *Computing*, 64:323–338, 2000.

[27] I.W. Stewart. *The Static and Dynamic Continuum Theory of Liquid Crystals: A Mathematical Introduction*. Taylor and Francis, London, 2004.

[28] E.G. Virga. *Variational Theories for Liquid Crystals*. Chapman and Hall, London, 1994.

[29] H. Wu, X. Xu, and C. Liu. On the general Ericksen-Leslie system: Parodi's relation, well-posedness and stability. *Arch. Rational Mech. Anal.*, pages 59–107, 2013.

[30] H. Zocher. Über die Einwirkung magnetischer, elektrischer und mechanischer Kräfte auf Mesophasen. *Physik. Zietschr.*, 28:790–796, 1927.